



ELSEVIER

Contents lists available at ScienceDirect

## Journal of Sound and Vibration

journal homepage: [www.elsevier.com/locate/jsv](http://www.elsevier.com/locate/jsv)

# An automatic mode pairing strategy using an enhanced modal assurance criterion based on modal strain energies

Maik Brehm<sup>a,\*</sup>, Volkmar Zabel<sup>a</sup>, Christian Bucher<sup>b</sup>

<sup>a</sup> Bauhaus-University Weimar, Institute of Structural Mechanics, Marienstrasse 15, 99423 Weimar, Germany

<sup>b</sup> Vienna University of Technology, Center of Mechanics and Structural Dynamics, Karlsplatz 13, A-1040 Wien, Austria

## ARTICLE INFO

### Article history:

Received 27 July 2009

Received in revised form

4 July 2010

Accepted 7 July 2010

Handling Editor: K. Shin

## ABSTRACT

In the context of finite element model updating using output-only vibration test data, natural frequencies and mode shapes are used as validation criteria. Consequently, the correct pairing of experimentally obtained and numerically derived natural frequencies and mode shapes is important. In many cases, only limited spatial information is available and noise is present in the measurements. Therefore, the automatic selection of the most likely numerical mode shape corresponding to a particular experimentally identified mode shape can be a difficult task. The most common criterion for indicating corresponding mode shapes is the modal assurance criterion. Unfortunately, this criterion fails in certain cases and is not reliable for automatic approaches.

In this paper, the purely mathematical modal assurance criterion will be enhanced by additional physical information from the numerical model in terms of modal strain energies. A numerical example and a benchmark study with experimental data are presented to show the advantages of the proposed energy-based criterion in comparison to the traditional modal assurance criterion.

© 2010 Elsevier Ltd. All rights reserved.

## 1. Introduction

The updating of finite element models with respect to experimentally obtained data has been in the focus of research for several years. Many approaches developed in this context use modal parameters, in particular natural frequencies and mode shapes, that are identified from data acquired during dynamic tests as a measure of model quality (e.g., [1]). This usually results in the formulation of an optimization problem that tries to minimize the difference between natural frequencies and mode shapes calculated for a finite element model and those identified experimentally. To achieve this goal, several objective functions were developed and described in the literature (e.g., [2–4]). Regardless of which objective function based on modal information is applied in a specific study, the success of optimization strongly depends on a reliable assignment of numerical modes to the respective experimentally obtained modes. This can be a challenge not only because of changes in the order of mode shapes due to a change of model parameters, but also due to the fact that only a limited number of degrees of freedom are included in experimentally obtained mode shapes.

Most mode assignment strategies are based on criteria that were developed to investigate the correlation between an experimentally identified modal vector and the respective mode shape of a numerical model. These indicators were developed by several authors and are described in standard text books on experimental modal analysis such as [5–7].

One of these measures for the correlation of two mode shapes is the modal scale factor (MSF), originally developed in [8]. This measure is a non-normalized indicator that depends on the scaling of two vectors. Accordingly, the magnitude of the MSF is strongly related to the applied normalization that is used in the analysis which can cause problems in context with a correct

\* Corresponding author. Tel.: +49 3643 584507; fax: +49 3643 584514.

E-mail addresses: [maik.brehm@uni-weimar.de](mailto:maik.brehm@uni-weimar.de) (M. Brehm), [volkmar.zabel@uni-weimar.de](mailto:volkmar.zabel@uni-weimar.de) (V. Zabel), [christian.bucher@tuwien.ac.at](mailto:christian.bucher@tuwien.ac.at) (C. Bucher).

assignment of respective modes. The most widely used approach to check the correlation between experimental and numerical modal vectors is the modal assurance criterion (MAC). It was introduced in [8] and has been discussed in several Refs. (e.g., [9,10]) as well as in the aforementioned text books. The main advantages of the MAC are its straightforward implementation, as it does not require coordinate-complete experimental eigenvectors or system matrices [11], and its independence of the scaling of mode shapes. The possible range of the MAC is from zero to one. An application of the MAC in the context of topology optimization using reduced nodal information is given in [12]. Another criterion that is related to both the MAC and the MSF was suggested in [13,6]. It is based on normalized modal differences (NMD) and indicates maximal correlation by zero. It is not bounded and yields to infinity in the case of perfect orthogonal mode shapes, which can be a drawback in practice.

Several other correlation measures are based on the MAC. For example, the linear modal assurance criterion (LMAC), proposed by [11], linearizes the nonlinear behavior of the MAC. This results in a higher sensitivity in case of almost identical modal vectors. The coordinate modal assurance criterion (COMAC) [14] and ECOMAC [15] highlight the discrepancy of particular degrees of freedom and require a preliminary mode pairing. An overview and further discussion is given in [9,11]. The weighted modal assurance criterion, or normalized cross orthogonality (NCO), [16,5,11] includes additional physical information of the structure by using reduced or expanded mass or stiffness matrices of a finite element model. Ref. [11] discussed this measure and indicated advantages compared to the MAC. However, a disadvantage is the generation of additional errors and inaccuracies due to the necessary reduction or expansion procedure.

Unfortunately, the previously described criteria tend to fail under certain, but typical, conditions. There are cases where a defined sensor setup can only capture the global dynamic behavior but not local modes, such as vibrations of certain structural elements or substructures. If one considers, for example, a space frame structure where sensors were placed at the structural nodes, the global bending and torsional modes of the system can be identified very well, but not the mode shapes of the truss rods. Due to small modal displacements of local modes at the measured global positions of the structure, artificial modes could be detected which can influence a correct mode assignment. Another example could be an arch bridge, where only the bridge deck may be accessible for vibration measurements but not the arch. Here, it can become very difficult to distinguish between the modes of the arch and the modes of the deck. This is explained to a certain extent by the existence of vibration modes of the arch for which the bridge deck shows a similar vibration shape as for a bending or torsional mode of the bridge deck [17].

These problems arise mainly if the spacial information in the experimentally identified mode shapes is incomplete. In an interactive analysis, the recognition of correct mode assignment can be managed in many cases by engineering judgment. However, an automated process such as an optimization or a sensitivity analysis in context with finite element model updating requires a different approach.

The main emphasis of this paper is given to situations where the mode correlation criteria mentioned may fail in the correct assignment of numerical to experimental modes due to incomplete spacial information in the experimental data. The paper presents a novel mode assignment strategy that enhances the purely mathematical modal assurance criterion (MAC) by physical information about stiffness distributions which in the case of using mass-normalized eigenvectors leads to a relation with modal strain energies of numerically obtained mode shapes. Therefore, the new criterion is called the energy-based modal assurance criterion (EMAC). Typical applications are systems where only unidirectional measurements are possible. The proposed methods can also be applied to systems with several weakly coupled substructures, for which sufficient modal information is not available for all substructures. The developed method is suitable to be applied for an automatic mode assignment, for example, within an optimization procedure.

Even though modal strain energies have been applied to manifold problems, their use in combination with mode assignment, as presented in this paper, is novel. For example, various approaches that use modal strain energies to detect and locate structural damage are described in the literature (e.g., [18–21]). In [22], it is suggested applying modal strain energies to select the most relevant modes with respect to certain structural damage that are taken into account in model updating to detect and localize damage. Also in context with damage detection, an approach is suggested in [23] that uses measured modal strains to derive modal curvatures which are used as a damage indicator. Some of these approaches require a numerical model of the considered structure that has to describe the respective structural behavior with sufficient accuracy. This is usually obtained by updating the parameters of an initial model. If the available experimental modes are spatially incomplete, especially for systems with several substructures, the correct assignment of the respective modes is of great importance to the updating process.

For the sake of enhanced understanding, the theory of the most relevant mode pairing criteria is briefly described in the following section, before the suggested criterion is defined. A numerical benchmark study and an experimental case study are presented, where the suggested approach leads to satisfying results with limited additional numerical effort while the application of the modal assurance criterion (MAC) fails to find the correct mode shapes.

## 2. Review of the most important existing mode pairing criteria

### 2.1. Modal assurance criterion (MAC)

According to [8], the modal assurance criterion (MAC) is defined as

$$MAC_{ij} = \frac{(\hat{\Phi}_i^T \hat{\Phi}_j)^2}{(\hat{\Phi}_i^T \hat{\Phi}_i)(\hat{\Phi}_j^T \hat{\Phi}_j)}, \quad (1)$$

where  $\hat{\Phi}_j$  is the reduced numerical eigenvector of mode  $j$  containing only the measured degrees of freedom.  $\hat{\Phi}_i$  is the corresponding experimental eigenvector of the experimental derived mode  $i$ . The modal assurance criterion is a purely mathematical criterion for checking the consistency between two eigenvectors.  $MAC_{ij} = \max_j(MAC_{ij})$  assigns the  $J$ th numerical mode to the experimental mode  $i$ . For perfectly correlated mode shapes that are in an appropriate order, the indices  $i$  and  $J$  should agree with each other. As long as the modes are evidently separated based on the available sparse spatial information and the measurement noise is negligible, the modes can be assigned with high reliability. Some applications can be found in [24,12,22].

According to [11], the linearized version of the MAC, the linear modal assurance criterion (LMAC) is formulated by

$$LMAC_{ij} = 1 - \frac{2}{\pi} \arccos \sqrt{MAC_{ij}} \quad \text{with} \quad \arccos \sqrt{MAC_{ij}} = \left[0, \frac{\pi}{2}\right]. \tag{2}$$

The possible values of the MAC and the LMAC range between zero and one, where one indicates a perfect fit. Ref. [11] shows that the LMAC becomes more sensitive if two modes are almost identical. Advantages of the MAC and the LMAC are convenient implementation and their independence of system matrices. The MAC and the LMAC do not consider system properties like inhomogeneous mass or stiffness distribution [9]. Therefore, the application in those cases is not recommended.

### 2.2. Normalized cross orthogonality (NCO)

An extension of the MAC is the weighted modal assurance criterion (WMAC) [9], also denoted as modified MAC (ModMAC) [25] or normalized cross orthogonality (NCO) check, proposed by [16,10]. This normalized cross orthogonality is given by

$$NCO_{ij} = \frac{(\hat{\Phi}_i^T \mathbf{W} \hat{\Phi}_j)^2}{(\hat{\Phi}_i^T \mathbf{W} \hat{\Phi}_i)(\hat{\Phi}_j^T \mathbf{W} \hat{\Phi}_j)}, \tag{3}$$

where  $\mathbf{W}$  is a weighting matrix. Usually, either the mass or the stiffness matrix of the numerical model are used as weighting matrix [16,25,11,10]. If the mass matrix is applied, those modal components that are related to high kinetic energy contributions are accentuated while the application of the stiffness matrix highlights the high strain energy contributions [25]. Since usually only limited information about the total degrees of freedom is available from tests, reduced system matrices have to be used. It has to be recognized that a reduction of the system matrices introduces additional errors into the system. A frequently used method to generate reduced system matrices is the Guyan reduction, also called static condensation [26]. The numerical effort increases with a smaller ratio between known and unknown DOF, which can be critical for some applications. A numerically more efficient method—the system equivalent reduction and expansion process (SEREP)—has been proposed by [27,28] and is briefly explained in [5]. The condensed mass matrix  $\mathbf{M}_a^S$  and the condensed stiffness matrix  $\mathbf{K}_a^S$  are calculated by

$$\mathbf{M}_a^S = \mathbf{T}^T \mathbf{M} \mathbf{T} \quad \text{and} \quad \mathbf{K}_a^S = \mathbf{T}^T \mathbf{K} \mathbf{T}. \tag{4}$$

The full size mass and stiffness matrices are denoted by  $\mathbf{M}$  and  $\mathbf{K}$ , respectively.

The transformation matrix  $\mathbf{T} = \Phi \hat{\Phi}^+$  is given by the numerical eigenvector matrix  $\Phi$  with dimension of the numerical model and the generalized inverse of the reduced eigenvector matrix  $\hat{\Phi}$ . If  $\hat{\Phi}$  consists of  $a$  independent rows (measured DOFs) and  $m$  independent columns (number of considered modes), the generalized inverse  $\hat{\Phi}^+$  can be calculated using the singular value decomposition  $\hat{\Phi} = \mathbf{L} \mathbf{S} \mathbf{R}^T$  [10] as  $\hat{\Phi}^+ = \mathbf{R} \mathbf{S}^+ \mathbf{L}^T$ .

Assuming the weighting matrix of Eq. (3) is given by a SEREP-condensation, the normalized cross orthogonality is also referred to as SEREP cross orthogonality (SCO) [10].

An extension similar to the linearized modal assurance criterion has been proposed by [11]

$$LNCO_{ij} = 1 - \frac{2}{\pi} \arccos \sqrt{NCO_{ij}} \quad \text{with} \quad \arccos \sqrt{NCO_{ij}} = \left[0, \frac{\pi}{2}\right]. \tag{5}$$

The values of NCO and LNCO range between zero and one. One indicates a perfect fit.

### 3. Mode assignment using energy-based modal assurance criterion

In the case of a mass normalized modal matrix  $\Phi$ , where the  $j$ th column corresponds to the eigenvector of the  $j$ th eigenvalue  $\omega_j^2$ , one has

$$\Phi^T \mathbf{M} \Phi = \mathbf{I} \tag{6}$$

and

$$\Phi^T \mathbf{K} \Phi = \text{diag}(\omega_j^2) \tag{7}$$

with the mass matrix  $\mathbf{M}$ , stiffness matrix  $\mathbf{K}$ , and identity matrix  $\mathbf{I}$ . According to Eq. (7), the total modal strain energy for each mode  $j$  is  $\frac{1}{2} \omega_j^2$ . By separating the available degrees of freedom into  $n$  clusters, the eigenvector of mode  $j$  can be

rewritten as

$$\Phi_j^T = [\Phi_{j1}^T \ \Phi_{j2}^T \ \dots \ \Phi_{jn}^T]^T. \quad (8)$$

The corresponding clustered stiffness matrices  $\mathbf{K}_{kl} \forall k, l = 1, 2, \dots, n$  are then given by

$$\mathbf{K} = \begin{bmatrix} \mathbf{K}_{11} & \mathbf{K}_{12} & \dots & \mathbf{K}_{1n} \\ \mathbf{K}_{21} & \mathbf{K}_{22} & \dots & \mathbf{K}_{2n} \\ \vdots & \vdots & \ddots & \vdots \\ \mathbf{K}_{n1} & \mathbf{K}_{n2} & \dots & \mathbf{K}_{nn} \end{bmatrix}. \quad (9)$$

Hence, the modal strain energy for mode  $j$  with respect to cluster  $k$  is obtained

$$\text{MSE}_{jk} = \frac{1}{2} \sum_{l=1}^n \Phi_{jk}^T \mathbf{K}_{kl} \Phi_{jl}. \quad (10)$$

Accordingly, the total strain energy of mode  $j$  is represented by

$$\text{MSE}_j = \frac{1}{2} \sum_{k=1}^n \sum_{l=1}^n \Phi_{jk}^T \mathbf{K}_{kl} \Phi_{jl} = \frac{1}{2} \Phi_j^T \mathbf{K} \Phi_j = \frac{1}{2} \omega_j^2. \quad (11)$$

Eqs. (10) and (11) yield to the relative modal strain energy of mode  $j$  with respect to cluster  $k$ :

$$\Pi_{jk} = \frac{\text{MSE}_{jk}}{\text{MSE}_j} = \frac{\sum_{l=1}^n \Phi_{jk}^T \mathbf{K}_{kl} \Phi_{jl}}{\Phi_j^T \mathbf{K} \Phi_j} \quad \text{with } \text{MSE}_j \neq 0. \quad (12)$$

Therefore, extending Eq. (1) by Eq. (12) yields to an energy-based modal assurance criterion for each cluster  $k$ :

$$\text{EMAC}_{ijk} = \Pi_{jk} \text{MAC}_{ij}. \quad (13)$$

Based on the linearized modal assurance criterion (LMAC), an equivalent energy-based linear modal assurance criterion can be defined

$$\text{ELMAC}_{ijk} = \Pi_{jk} \text{LMAC}_{ij}. \quad (14)$$

The assignment of modes is given similarly to the modal assurance criterion, where the numerical mode with the largest value is assigned to the respective experimental mode. The relative modal strain energy  $\Pi_k$ , which is in the range between zero and one, and the modal assurance criterion (MAC) are connected by multiplication. Therefore, the range of the energy-based modal assurance criterion EMAC is bounded between zero and one. The relative modal strain energy of the observed cluster reflects the amount of energy which can be covered by the measurements. By this interpretation, the EMAC involves both, the possibility that a numerical mode can be represented by the measurements and by the purely mathematical correlation between scaled measured and scaled numerical modes.

Of course, the success of this method depends on the selected numerical degrees of freedom which will be clustered. Since this selection strongly depends on the specific structure to be investigated and the experimental setup used, it is difficult to give a general guideline. However, the clusters should be chosen such that the measured degrees of freedom can be separated from those degrees of freedom that were not considered in the tests. In the case of the presence of substructures, the selection of clusters should also be related to the substructures. For a better understanding of this problem, examples of typical cases are given in the following section.

## 4. Benchmark study: cantilever truss

### 4.1. Description of the system

The numerical example is based on a 20 degree of freedom cantilever beam consisting of 12 nodes and 21 truss members. It has been used in [29] for a numerical model updating benchmark. The geometry is presented in Fig. 1. The cross-sectional area and the mass density of all truss members are defined to  $0.03 \text{ m}^2$  and  $2700 \text{ kg/m}^3$ , respectively. The material is linearly elastic with Young's modulus of  $7 \times 10^{10} \text{ N/m}^2$ .

For the numerical test example, it is assumed that the vertical modal displacements at the four measurement points (MP), indicated in Fig. 1, are available for identifying the first four vertical modes. The corresponding mode shapes are shown in Fig. 2. Furthermore, it is assumed that the mode shapes, supposed to be identified from tests, are affected by some inaccuracies. These inaccuracies are simulated by adding normally distributed perturbations with a mean value of 0 and a coefficient of variation of 0.05 to the calculated modal displacements. These noise disturbed mode shapes are referred to as experimental mode shapes in the following. The original modal displacements and one set of random perturbations of noisy modal displacements are given in Tables 1 and 2, respectively.

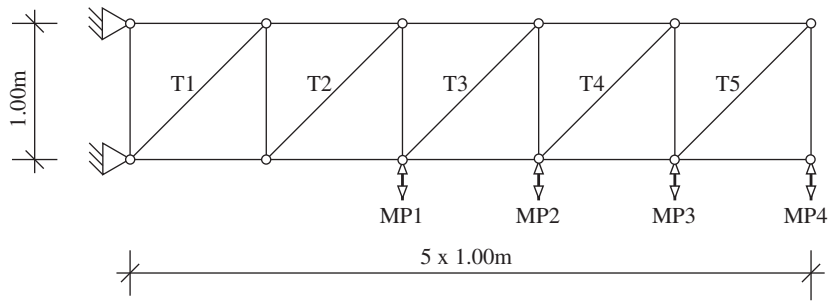


Fig. 1. Geometrical description of the cantilever truss system.

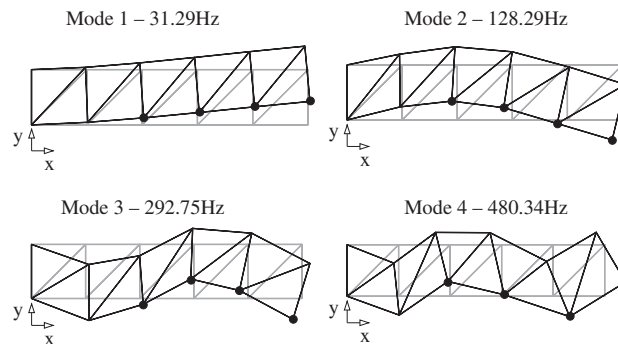


Fig. 2. First four “measured” vertical mode shapes of the system obtained by simulation. Only the vertical modal displacements of the marked positions (●) are assumed to be available from tests.

#### 4.2. Application of mode assignment

It is assumed that a design of an optimization run or a sample of a sensitivity analysis leads to a change of Young's moduli of the diagonal elements T2 and T4 to  $2.2 \times 10^{11}$  N/m<sup>2</sup>. The first nine modes of the changed system are presented in Fig. 3. For reliable results in the subsequent analyses, it is essential that the experimentally obtained modes are assigned to the most likely numerical modes based only on the vertical modal displacements of the four measurement points. The MAC values between numerical and noise disturbed experimental modes are presented in Fig. 4. It can be observed that the MAC values between the second experimental mode and the second and third numerical modes are close to 1 which indicates an almost perfect agreement in both cases. If the original MAC is used to select the mode, the wrong third numerical mode, which is mainly a longitudinal mode, will be assigned to the second experimental mode, because the MAC value is slightly larger. The results are given in Figs. 5 and 6. This wrong mode assignment can cause essential problems for some investigations, for example, the sensitivity analysis or model updating.

The proposed alternative approach uses the relative modal strain energy to pair correct modes. Therefore, the total degrees of freedom are separated into two clusters. Cluster 1 contains the vertical degrees of freedom and cluster 2 contains the horizontal degrees of freedom. The relative modal strain energies  $II_{jk}$  according to Eq. (12) are visualized in Fig. 7. By this criterion, the modes can be distinguished into primary horizontal and primary vertical modes. The EMAC according to Eq. (13) is presented in Fig. 8. The largest value in each row indicates to which numerical mode the respective experimental mode has to be assigned. The EMAC and the original MAC of the identified modes are shown in Figs. 9 and 10, respectively. Fig. 11 presents the selected numerical mode shapes. It can be observed that the correct second numerical mode can be assigned to the second experimental mode.

This numerical benchmark study shows that the MAC is able to pair the correct modes as long as the modes can be reliably separated based on the sparse spatial information. If the modes cannot be separated by the available information, the physical information of the modes, namely the modal strain energy, can be used to distinguish between modes with similar MAC values.

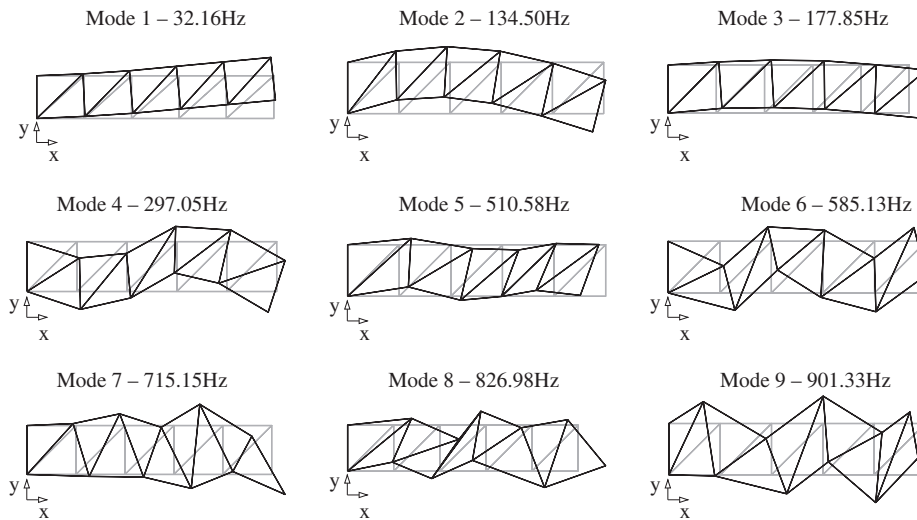
Obviously, the size of perturbation is essential for the success of the investigated mode assignment criteria. Therefore, the coefficient of variation which determines the size of perturbation is varied by 2, 5, and 10 percent. For each value, 1000 samples are generated based on a normal distribution using the Monte Carlo method. Table 3 shows the success of both mode assignment criteria, MAC and EMAC. It can be observed that the EMAC is very robust and is always able to assign the right modes. The MAC criterion shows good results for the lowest level of perturbations. However, with increasing size of

**Table 1**  
Original modal displacements.

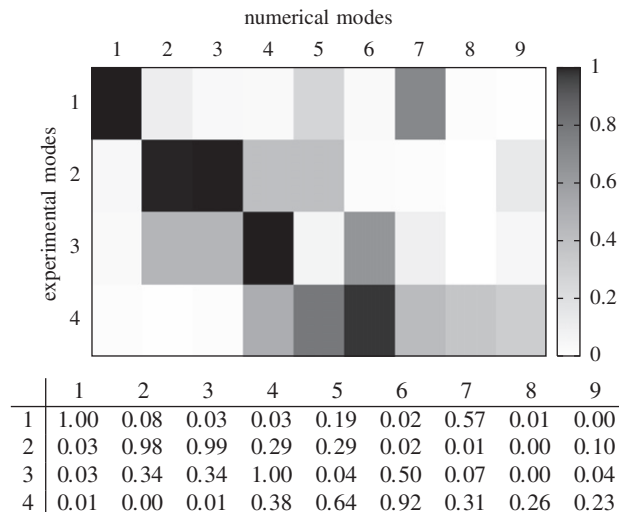
	Mode 1	Mode 2	Mode 3	Mode 4
MP1	-0.0127	0.0344	0.0107	0.0287
MP2	-0.0225	0.0224	-0.0360	0.0029
MP3	-0.0327	-0.0064	-0.0149	-0.0395
MP4	-0.0425	-0.0362	0.0384	0.0275

**Table 2**  
Perturbations of modal displacements.

	Mode 1	Mode 2	Mode 3	Mode 4
MP1	0.0010	0.0007	-0.0001	-0.0015
MP2	-0.0002	0.0043	-0.0001	-0.0002
MP3	-0.0004	-0.0003	-0.0002	0.0016
MP4	-0.0012	0.0041	0.0016	-0.0014



**Fig. 3.** First nine mode shapes of the modified numerical model.



**Fig. 4.** Modal assurance criterion (MAC)—numerical vs. experimental modes.

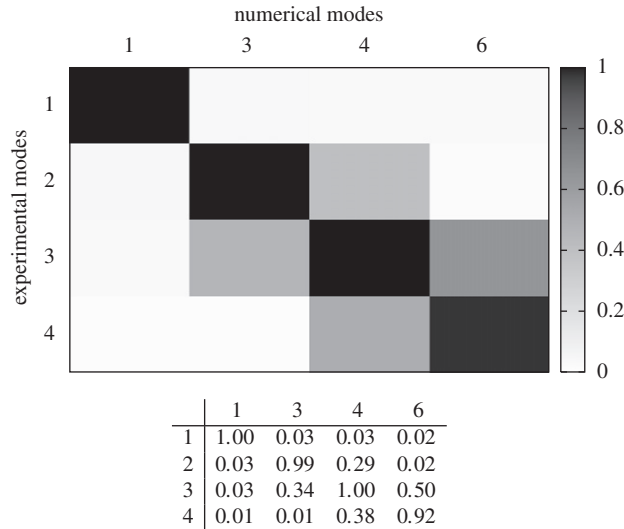


Fig. 5. Modal assurance criterion (MAC)—identified numerical vs. experimental modes.

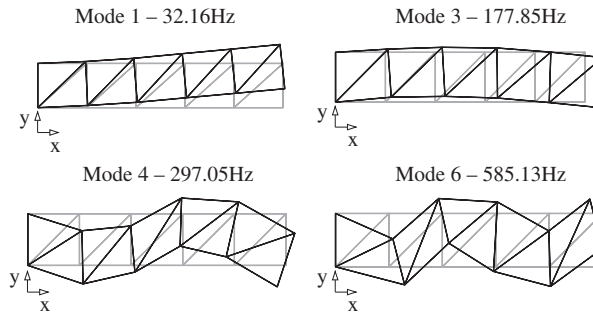


Fig. 6. Identified mode shapes from numerical modal analysis using MAC.

perturbations, the possibility of getting a failed mode assignment increases by using the MAC criterion. For a coefficient of variation of 10 percent, more than 20 percent of the mode assignments failed.

However, the success of using the MAC as mode pairing criterion in the presented benchmark study depends strongly on the size and distribution of the perturbations itself, while the success of the proposed EMAC is less sensitive to a commonly acceptable size of perturbations.

### 4.3. Optimization

Assuming that only Young’s moduli of the diagonal element T2 and T4 are unknown, an optimization problem can be established. Young’s moduli are defined by  $E(T 2)=7k_2 \times 10^{10} \text{ N/m}^2$  and  $E(T 4)=7k_4 \times 10^{10} \text{ N/m}^2$ , respectively. Based on the values  $k_2=1$  and  $k_4=1$ , the artificial experimentally derived modal parameters are defined and presented in Fig. 2. The subsequently applied measured, noise disturbed, modal displacements are obtained by adding the perturbations given in Table 2 to the original values of Table 1. Hence, the measured feature vector

$$\mathbf{z}_m = [f_1 \ f_2 \ f_3 \ f_4 \ 1 \ 1 \ 1 \ 1]^T \tag{15}$$

is assembled by the first four measured known natural frequencies  $f_i$  and the four values of 1 assuming the best value for the MAC of the first four paired modes. The updated feature vector is given by

$$\mathbf{z}_p = [f_{1,p} \ f_{2,p} \ f_{3,p} \ f_{4,p} \ \text{MAC}_{11,p} \ \text{MAC}_{22,p} \ \text{MAC}_{33,p} \ \text{MAC}_{44,p}]^T, \tag{16}$$

where  $f_{i,p}$  are the four updated numerical natural frequencies at optimization step  $p$  obtained by the mode pairing strategy. The MAC is based on the four measured modes and the corresponding identified numerical modes. The objective function

$$g = \sqrt{(\mathbf{z}_m - \mathbf{z}_p)^T \mathbf{W} (\mathbf{z}_m - \mathbf{z}_p)} \quad \text{with } g(\mathbf{z}_p(\theta_p)) \rightarrow \min \tag{17}$$

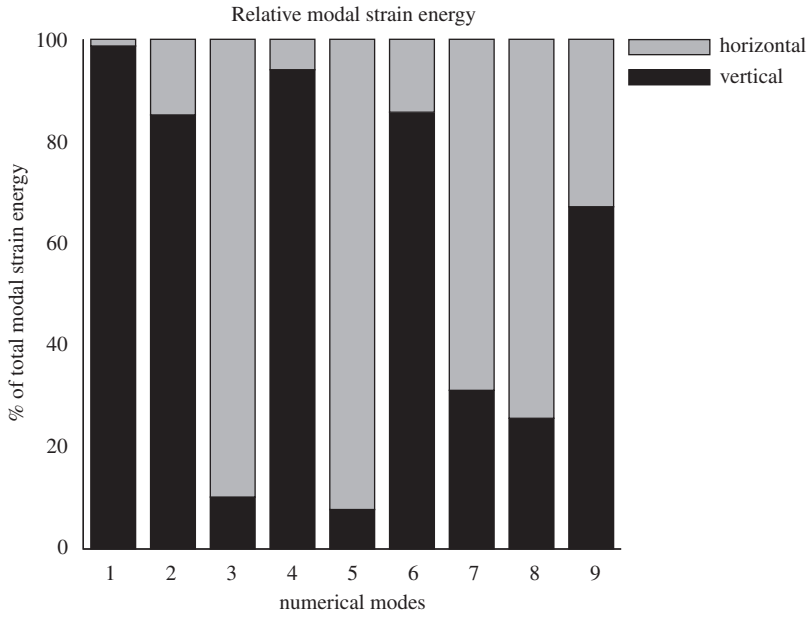


Fig. 7. Relative modal strain energies for vertical and horizontal degrees of freedom.

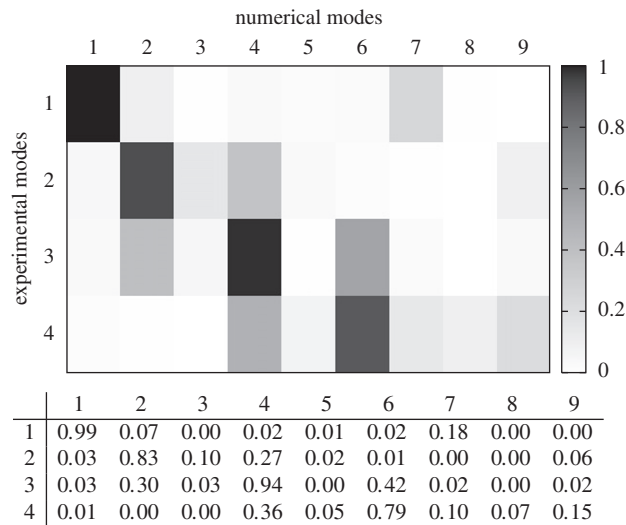


Fig. 8. Energy-based modal assurance criterion (EMAC) for vertical degrees of freedom—numerical vs. experimental modes.

is based on the weighted Euclidean distance between the measured feature vector  $\mathbf{z}_m$  and the updated feature vector  $\mathbf{z}_p$ , whereas  $\mathbf{z}_p$  depends on the unknown parameters  $\theta_p = [k_2 \ k_4]^T$ . The weighting matrix  $\mathbf{W}$  is a diagonal matrix defined by

$$\mathbf{W} = \text{diag}(f_1^{-2}, f_2^{-2}, f_3^{-2}, f_4^{-2}, 1, 1, 1, 1). \tag{18}$$

The initial estimates for the optimization are  $\theta_0 = [1.05 \ 0.90]^T$ .

Using an adaptive response surface approach (e.g., [30,31]), where the optimization at the approximated surfaces is based on a combination of the gradient-based method SQP (sequential quadratic programming) and genetic algorithm (GA) [32,33], optimal values can be obtained for  $\theta_p$ . The optimization method is described in Appendix A. The results are independent from the starting values  $\theta_0$  within the given range.

In the case of applying the MAC-based mode pairing strategy, the optimal values  $\theta_p = [0.70182 \ 0.70768]^T$  were obtained, which do not reflect the nominal values  $[1.00000 \ 1.00000]^T$ . This effect is explained by an inappropriate mode assignment.



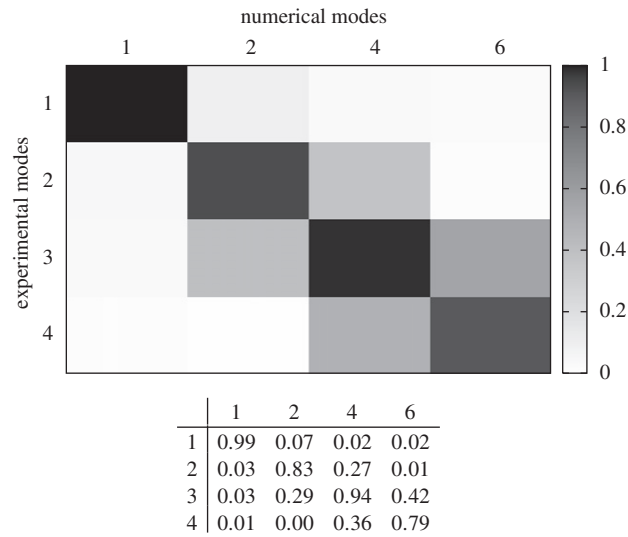


Fig. 9. Energy-based modal assurance criterion (EMAC) for vertical degrees of freedom—identified numerical vs. experimental modes.

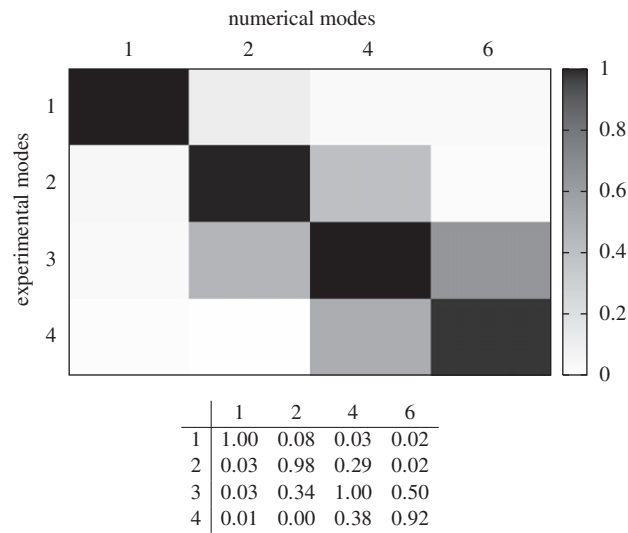


Fig. 10. Modal assurance criterion (MAC)—identified numerical vs. experimental modes. Numerical modes are previously selected by the energy-based modal assurance criterion (EMAC).

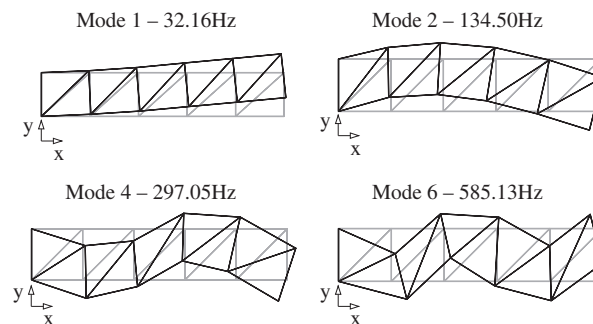
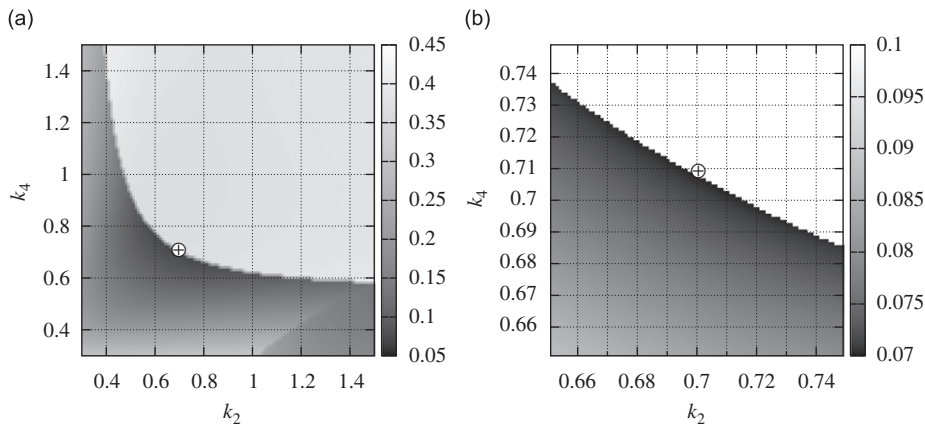


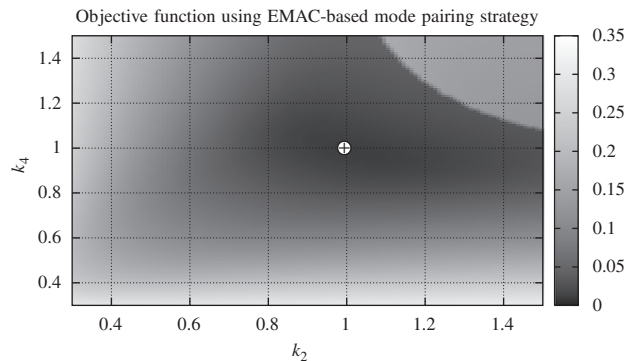
Fig. 11. Identified mode shapes from numerical modal analysis using the energy-based modal assurance criterion (EMAC).

**Table 3**  
Dependency of successful mode assignment on the level of noise.

Size of noise (coefficient of variation)	Mode assignment criterion	Assignment	
		Successful	Failed
0.02	MAC	1000	0
	EMAC	1000	0
0.05	MAC	920	80
	EMAC	1000	0
0.10	MAC	787	213
	EMAC	1000	0



**Fig. 12.** Objective function using MAC-based mode pairing strategy. The minimum is obtained at  $(k_2, k_4) = (0.70182, 0.70768)$  and marked by the white dot. Diagram (b) shows a detail of diagram (a).



**Fig. 13.** Objective function using EMAC-based mode pairing strategy. The minimum is obtained at  $(k_2, k_4) = (1.00010, 0.99994)$  and marked by the white dot.

Using the EMAC-based mode pairing strategy, the correct values  $\theta_p = [1.00010 \ 0.99994]^T$  were found. As the optimization itself is performed on the response surface, 250 objective function evaluations were required to define the supporting points for the response surface approximation. On a computer with an Intel Xeon 5130 (2.00 GHz) processor, the total computation time for the model updating is 10 min. The high number of objective function evaluations and total computation time is mainly related to the desired accuracy of the parameters. As in the previous study, the relative modal strain energies are related to all vertical degrees of freedom of the numerical model. The shapes of the objective functions are given in Figs. 12 and 13. The respective minima are marked by the white dot that coincides with the identified values. Accordingly, one can deduce that inaccurately identified values, in the case of formulating the objective function based on MAC-based mode assignment, are not caused by the choice of an inappropriate optimization strategy, but by the objective function itself. Note that the sharp edges in Figs. 12 and 13 indicate discontinuities in the objective functions due to mode switches. Furthermore, the optimum using the MAC-based approach is directly situated at the discontinuity of the

objective function, where the gradients in the vicinity of the optimum are small in the tangential direction of the edge, which is visualized in Fig. 12b. This causes a challenge for an optimization strategy.

These observations verify that the application of an inappropriate mode assignment strategy in a model updating algorithm can lead to wrong results for the optimization.

### 5. Case study: high-speed railway bridge EÜ Erfttalstraße

#### 5.1. Description of the system

The numerical model describes a high-speed railway bridge on the line between Cologne and Brussels, which has been discussed in several Refs. [34,35,4]. The filler beam bridge consists of two main superstructures, each carrying one rail line. The rail is installed on ballast that is continuously distributed over both superstructures and the transition zones between the bridge and the embankment. Figs. 14–16 show the simplified bridge model and the resulting finite element model.

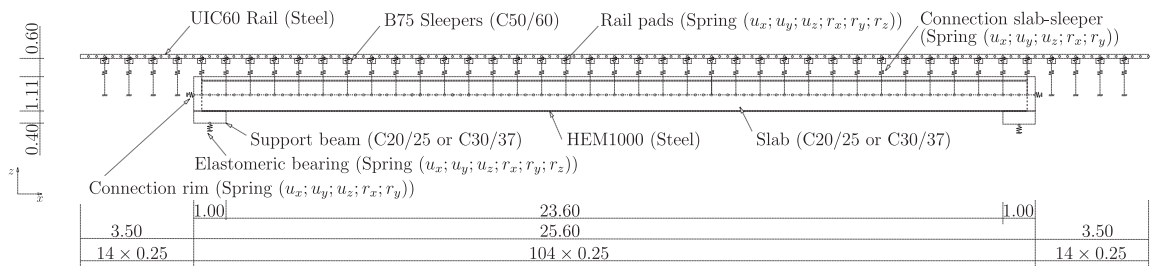


Fig. 14. Longitudinal section of the simplified bridge model.

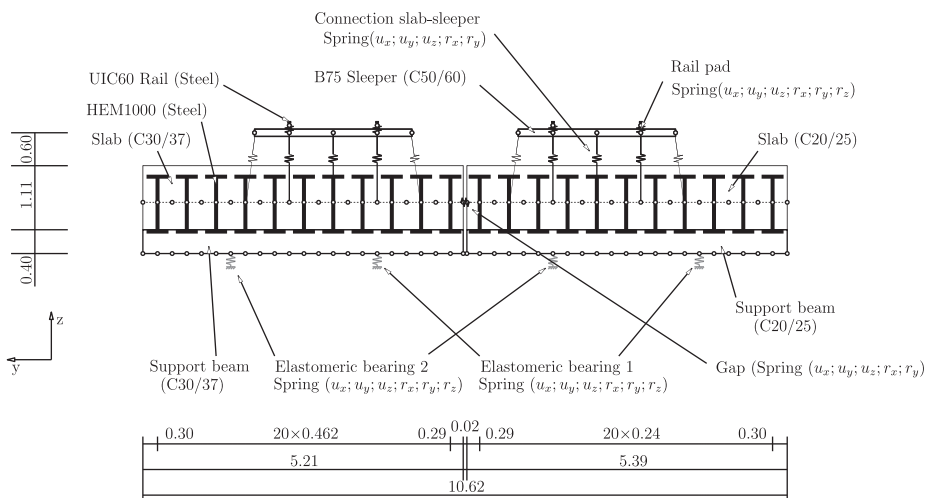


Fig. 15. Cross section of the simplified bridge model.

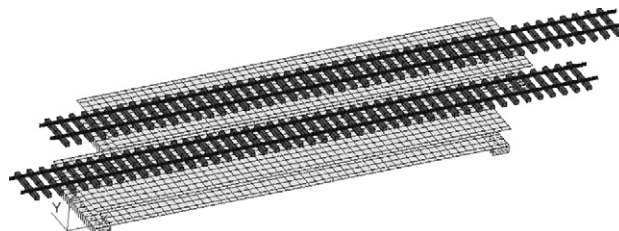


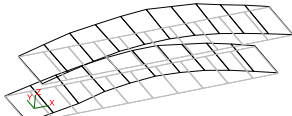


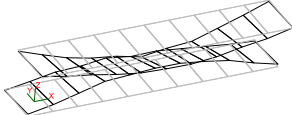
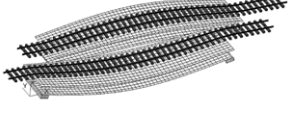
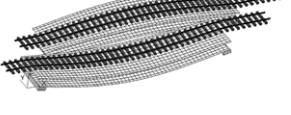
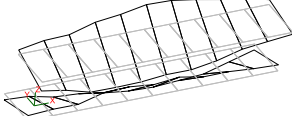
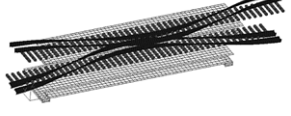
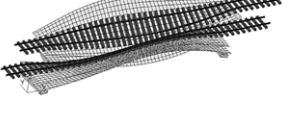
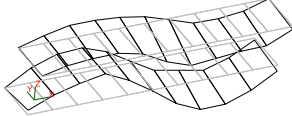
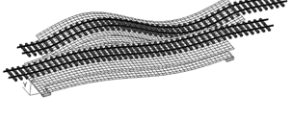
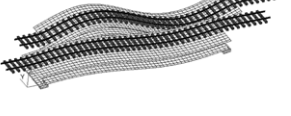
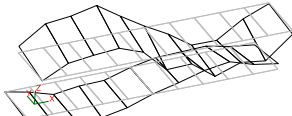
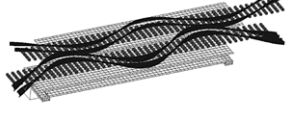

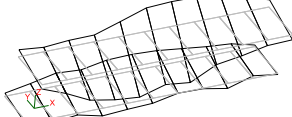
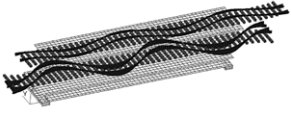
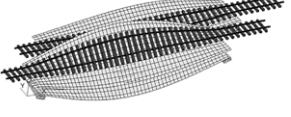
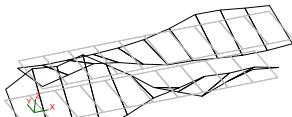
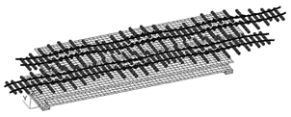

Fig. 16. Finite element model of the bridge.

A set of seven experimental mode shapes and corresponding natural frequencies were available from an experimental campaign which has been described in [35,4]. The mode shapes and the natural frequencies obtained from the experimental campaign are given in Table 4. Due to limitations in the experimental setup, the modal displacements are only available in vertical direction at 44 points at the bottom side of the composite slabs.

As the model is supposed to be used for model updating, a correct mode assignment is essential. A total number of 35 uncertain material parameters were initially defined. They are listed in Table 5.

**Table 4**

Comparison of identified numerical mode shapes with the mode shapes obtained from measurements.

	measured mode shape	numerical mode shape identified by	
		MAC	EMAC
1	3.67Hz 	3.67Hz 	3.67Hz 
2	5.24Hz 	5.82Hz 	5.82Hz 
3	9.36Hz 	7.28Hz 	15.14Hz 
4	13.17Hz 	12.69Hz 	12.69Hz 
5	13.71Hz 	14.38Hz 	13.89Hz 
6	15.09Hz 	18.86Hz 	18.38Hz 
7	20.98Hz 	31.41Hz 	30.75Hz 

**Table 5**

Notation, lower bounds, and upper bounds for the input variables.

#	Parameter	Unity	Lower bound	Upper bound
1	Young's m. concrete B25 including ballast	N/m <sup>2</sup>	$2.70 \times 10^{10}$	$4.50 \times 10^{10}$
2	Poisson ratio concrete B25 including ballast	–	$1.80 \times 10^{-1}$	$2.20 \times 10^{-1}$
3	Density concrete B25 including ballast	kg/m <sup>3</sup>	$3.00 \times 10^3$	$4.00 \times 10^3$
4	Young's m. concrete B25 including ballast	N/m <sup>2</sup>	$2.90 \times 10^{10}$	$4.50 \times 10^{10}$
5	Poisson ratio concrete B25 including ballast	–	$1.80 \times 10^{-1}$	$2.20 \times 10^{-1}$
6	Density concrete B25 including ballast	kg/m <sup>3</sup>	$3.00 \times 10^3$	$4.00 \times 10^3$
7	Young's m. HEM1000	N/m <sup>2</sup>	$2.00 \times 10^{11}$	$2.30 \times 10^{11}$
8	Poisson ratio HEM1000	–	$2.50 \times 10^{-1}$	$3.50 \times 10^{-1}$
9	Density HEM1000	kg/m <sup>3</sup>	$7.70 \times 10^3$	$8.00 \times 10^3$
10	Young's modulus sleeper	N/m <sup>2</sup>	$3.00 \times 10^{10}$	$5.00 \times 10^{10}$
11	Poisson ratio sleeper	–	$2.00 \times 10^{-1}$	$3.00 \times 10^{-1}$
12	Density sleeper	kg/m <sup>3</sup>	$2.10 \times 10^3$	$3.00 \times 10^3$
13	Shear m. elastomer 1	N/m <sup>2</sup>	$9.40 \times 10^6$	$4.50 \times 10^6$
14	Shear m. elastomer 2	N/m <sup>2</sup>	$9.40 \times 10^6$	$4.50 \times 10^6$
15	Ballast gap $u_x$	N/m	$3.00 \times 10^5$	$3.00 \times 10^{11}$
16	Ballast gap $u_y$	N/m	$5.00 \times 10^5$	$5.00 \times 10^{11}$
17	Ballast gap $u_z$	N/m	$3.00 \times 10^5$	$9.49 \times 10^7$
18	Ballast gap $r_x$	Nm/rad	$1.00 \times 10^1$	$1.00 \times 10^5$
19	Ballast gap $r_y$	Nm/rad	$1.00 \times 10^1$	$1.00 \times 10^8$
20	Ballast rim-soil $u_x$	N/m	$3.00 \times 10^4$	$3.00 \times 10^{11}$
21	Ballast rim-soil $u_y$	N/m	$5.00 \times 10^4$	$5.00 \times 10^{11}$
22	Ballast rim-soil $u_z$	N/m	$3.00 \times 10^5$	$3.00 \times 10^8$
23	Ballast rim-soil $r_x$	Nm/rad	$1.00 \times 10^1$	$1.00 \times 10^6$
24	Ballast rim-soil $r_y$	Nm/rad	$1.00 \times 10^1$	$1.00 \times 10^{10}$
25	Slab-sleeper $u_x$	N/m	$5.00 \times 10^4$	$5.00 \times 10^{11}$
26	Slab-sleeper $u_y$	N/m	$1.58 \times 10^5$	$5.00 \times 10^{11}$
27	Slab-sleeper $u_z$	N/m	$5.00 \times 10^5$	$5.00 \times 10^{11}$
28	Slab-sleeper $r_x$	Nm/rad	$1.00 \times 10^1$	$1.00 \times 10^5$
29	Slab-sleeper $r_y$	Nm/rad	$1.00 \times 10^1$	$1.00 \times 10^5$
30	Rail pad $u_x$	N/m	$1.00 \times 10^5$	$1.00 \times 10^{10}$
31	Rail pad $u_y$	N/m	$1.00 \times 10^5$	$1.00 \times 10^{10}$
32	Rail pad $u_z$	N/m	$5.01 \times 10^6$	$1.58 \times 10^9$
33	Rail pad $r_x$	Nm/rad	$1.00 \times 10^1$	$1.00 \times 10^5$
34	Rail pad $r_y$	Nm/rad	$1.00 \times 10^1$	$1.00 \times 10^5$
35	Rail pad $r_z$	Nm/rad	$1.00 \times 10^1$	$1.00 \times 10^5$

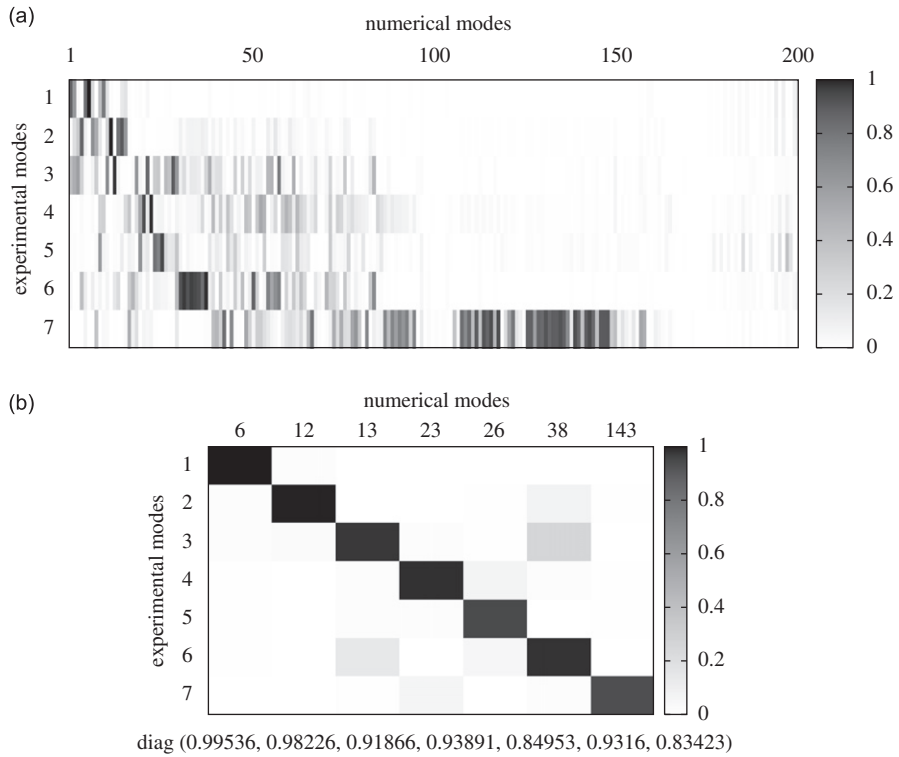
## 5.2. Application of mode assignment

One particular set of 35 unknown parameters was generated by a stochastic sampling scheme. For this set, a numerical modal analysis has been performed to extract the first 200 mode shapes and natural frequencies which represent a frequency range between 0 and 50 Hz. Many modes are primarily modes of the rail system containing a small modal deflection amplitude of the bridge deck. Due to noise influences, these modes are unlikely to be measured with the measured points at the bottom side of the slabs.

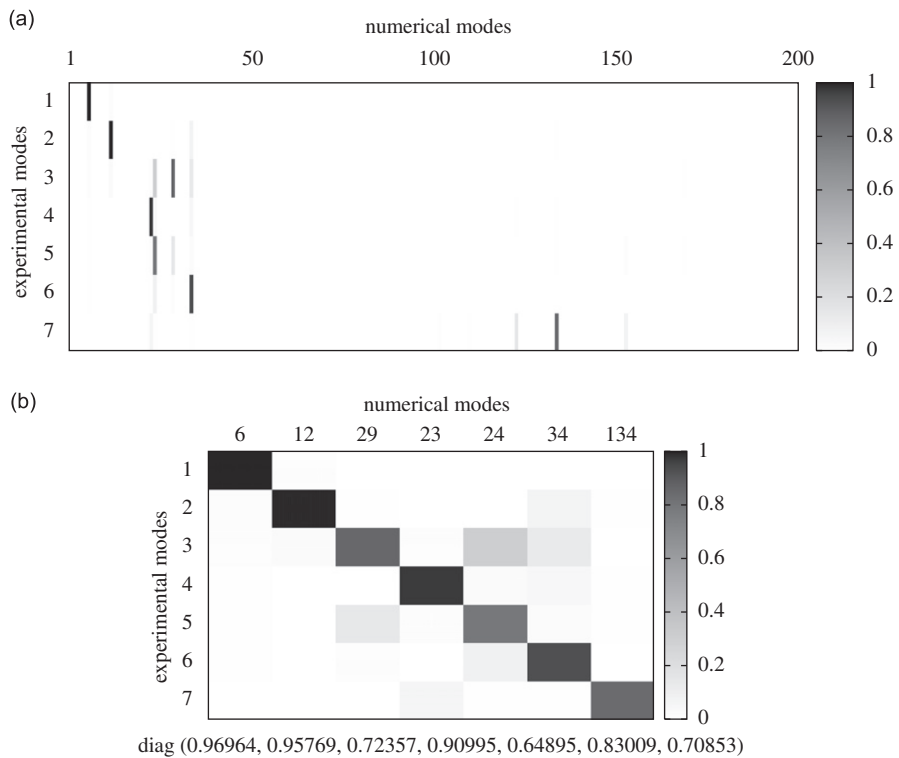
First, the original modal assurance criterion (MAC) will be used to assign the experimental to the corresponding numerical mode shapes. The MAC matrix for all 200 numerical and 7 experimental modes is given in Fig. 17a. The largest value in each row indicates the numerical mode which has to be assigned to the respective experimental mode. Based on this assignment, the MAC matrix, given in Fig. 17a, can be reduced. The reduced MAC matrix is presented in Fig. 17b. Because some MAC values between a certain measured mode and the numerical modes are almost identical, the selection is sensitive to noise and small changes in the input parameter values.

Alternatively, the energy-based modal assurance criterion (EMAC) will be used for mode assignment. As the sensors are homogeneously distributed at the bottom side of the main slabs in a vertical direction, the relative modal strain energies  $\Pi_{jk}$ , and therefore the corresponding EMAC values, are based on a cluster with all vertical degrees of freedom of the composite slabs with respect to the numerical model. The resulting EMAC matrix is visualized in Figs. 18a and b for the selected numerical modes. The MAC values for the selected numerical modes are illustrated in Fig. 19. It has been assumed that the main modal strain energy is present in the vertical components of the two main composite slabs. Since only one large EMAC value is present in each row, the selection is insensitive with respect to noise and small input parameter value changes.

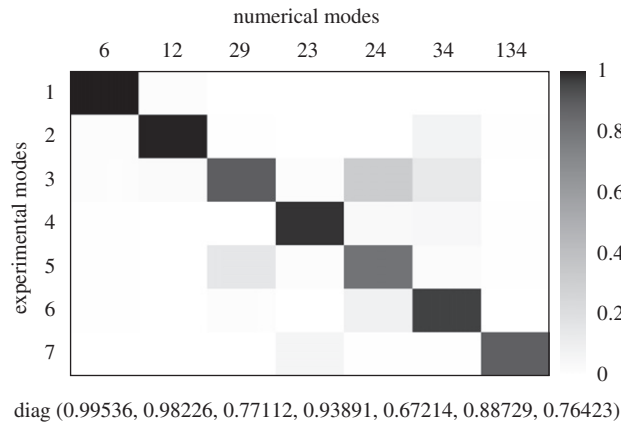
The compared mode selection methods, based on MAC and EMAC, assign some different numerical modes. The obtained modes are compared in Table 4. It should be noted that these numerical modes do not correspond to a model that was obtained by an optimization but with a parameter set that could be generated within one optimization step or during a sensitivity analysis. In the cases of measured modes 3, 5, 6, and 7, it can be observed that the assignment fails using the



**Fig. 17.** Modal assurance criterion (MAC)—(a) all numerical vs. experimental modes of the Erfttal bridge; (b) identified numerical vs. experimental modes of the Erfttal bridge.



**Fig. 18.** Energy-based modal assurance criterion (EMAC) for vertical degrees of freedom of the slab—(a) all numerical vs. experimental modes of the Erfttal bridge; (b) identified numerical vs. experimental modes of the Erfttal bridge.



**Fig. 19.** Modal assurance criterion—identified numerical vs. experimental modes of the Erfttal bridge. The numerical modes are selected previously by the energy-based model assurance criterion.

original MAC, whereas the EMAC values constitute a more reliable result. The main reason is the scaling of the MAC. It does not recognize the size of modal displacement compared to the largest modal displacement of a respective numerical mode of the complete system. Some of the primary rail modes have small modal deflections of the bridge decks, which are of similar shape as some of the global modes. Due to the lack of scaling of the reduced modal vectors, the MAC indicates an almost perfect fit.

For some parameter configurations and a certain level of noise, the MAC indicates a higher correlation between a global measured mode and a rail mode, which is an unlikely pairing. The proposed EMAC scales the MAC with the relative modal strain energy with respect to the vertical degrees of freedom of the bridge deck. Therefore, the rail modes with low relative modal strain energy will generate a small EMAC value. Finally, the EMAC is able to separate the modes and assigns the global numerical modes.

### 5.3. Global sensitivity analysis

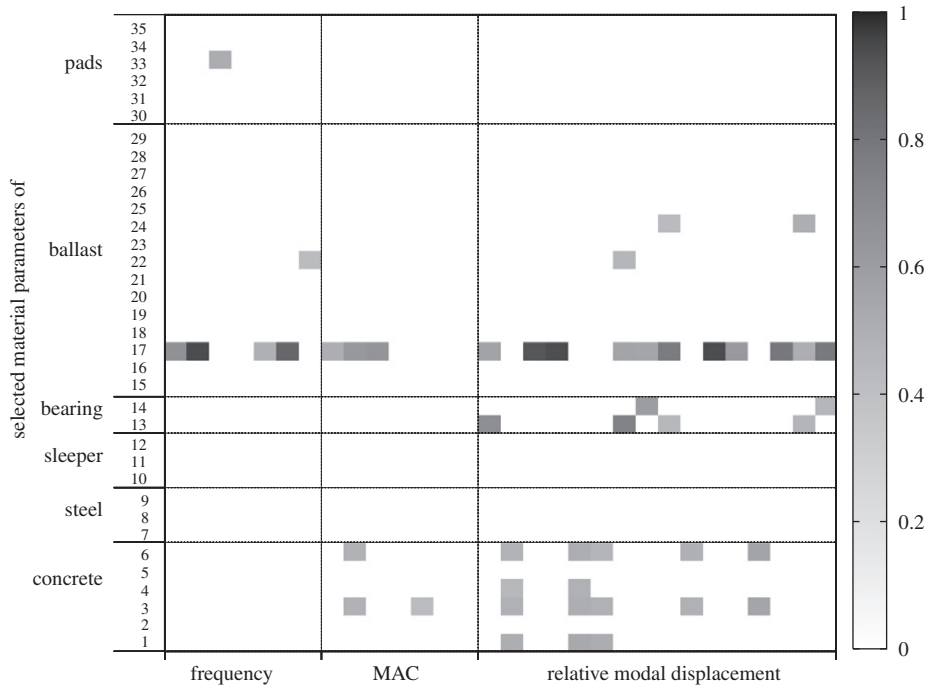
This analysis demonstrates the influence of an inappropriate mode selection algorithm on a global sensitivity analysis. The 35 selected, uncertain independent input parameters of the model were varied by a stochastic sampling scheme, the latin hypercube sampling. For each parameter, a uniform distribution is assumed. The boundaries are given in Table 5, where the numbering corresponds to the numbering of the vertical axis in Figs. 20 and 21. They are based on physically reasonable ranges. The latin hypercube sampling uses 750 classes, whereas one representative, the mean value, of each class will be selected. Therefore, the number of cubes is  $750^{35}$ . For all 750 generated sample sets, the modal parameters are calculated. All moduli of the linear Spearman correlation coefficient [36] between each input and output parameter pair were assembled into a matrix. The matrix was used to assess the sensitivity of each parameter with respect to a certain calculated modal parameter. Applications of the Spearman correlation in the context of model updating can be found in [37,38]. A compact theoretical description is given in Appendix B.

The assignment of numerical modes to the experimental modes is important. Fig. 20 shows the result when the traditional modal assurance criterion (MAC) is used for the mode assignment. By using the same design space, but applying the energy-based modal assurance criterion (EMAC) to the mode assignment, a different result was obtained, as presented in Fig. 21. For example, the MAC approach indicates a significant sensitivity of the bearings, which disappeared when the energy-based criterion was applied. Therefore, in the case of using the MAC, the sensitivity of the bearings is overvalued. As the most sensitive parameters should be used in the subsequent finite element model updating, a disadvantageous parameter will be used. This leads to an inaccurate identification of the bearing parameters and an unfavorable convergence rate within the optimization. By using the EMAC as mode pairing criterion, the bearing parameters will not be selected for finite element model updating.

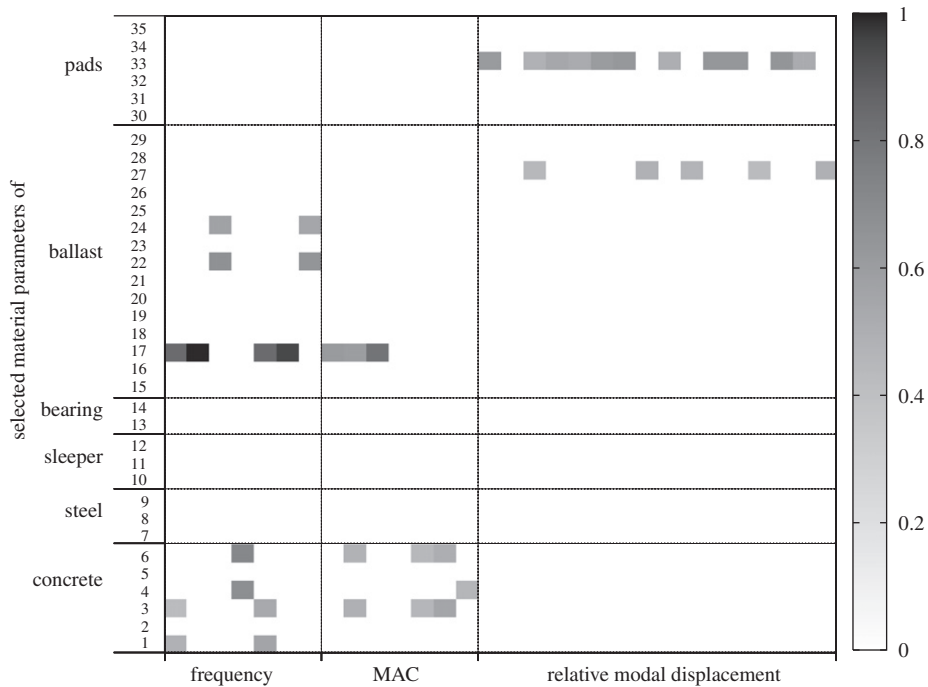
## 6. Discussion and conclusions

This paper emphasizes the problem of wrong mode selection by using the traditional modal assurance criterion (MAC) in certain cases. An innovative criterion combines the common mathematical modal assurance criterion with additional physical information, the modal strain energies of the numerical eigenvectors. This energy-based modal assurance criterion is denoted by EMAC. It has been shown that additional information leads to a more reliable mode assignment.

The problem has been explained extensively by means of a numerical example with artificially generated and noise disturbed measured data. It was shown that an optimization can lead to a wrong identification of parameters when using an inappropriate mode pairing algorithm. However, by applying the proposed EMAC, the most likely numerically derived



**Fig. 20.** Modulus of the linear Spearman correlation coefficient based on 750 sample sets using the modal assurance criterion (MAC) for mode assignment. Coefficients smaller than 0.3 are set to 0.



**Fig. 21.** Modulus of the linear Spearman correlation coefficient based on 750 sample sets using the energy-based modal assurance criterion (EMAC) for mode assignment. Coefficients smaller than 0.3 are set to 0.

modes could be assigned correctly to the respective experimentally determined mode. This is an important issue in the context of automated model updating that is focused on the correct identification of unknown model parameters. The proposed EMAC mode assignment has been tested on a high-speed railway bridge, for which experimentally identified



modal data were available. For the example of a single arbitrarily chosen parameter set of the finite element model of the bridge, it was shown that the most likely mode pairing was found by using the EMAC. The application of the MAC as mode pairing criterion failed in this case. Furthermore, the effect of a wrong mode assignment within a global sensitivity analysis became obvious.

An important step in the application of the energy-based modal assurance criterion (EMAC) is the selection of appropriate clusters, which is needed to define the relative modal strain energies. A general, detailed guideline for the selection of the clusters cannot be given, because the situation always depends on the specifics of each individual structure. The clusters always have to be defined depending on the kind of structure considered and the measurement setup used in the tests. In this context it is important,

1. that the degrees of freedom that are instrumented with sensors in the tests can represent the considered mode shapes sufficiently well and
2. that the selected clusters of the stiffness matrix have to be strongly related to those components of the numerical model that are known from the tests.

Finally, the proposed methodology cannot replace a careful preparation of modal tests. But it can significantly reduce uncertainties about the mode shapes in situations when only limited spacial information is available due to unavoidable reasons.

## Acknowledgments

The research presented in this article was carried out within the European project DETAILS (DEsign for opTimal assessment of high-speed rAILway bridges by enhanced monitoring Systems) that was supported by the European Research Fund for Coal and Steel (RFCS).

## Appendix A. Adaptive response surface method

The proposed adaptive response surface approach uses a combination of the gradient-based method SQP (sequential quadratic programming) and genetic algorithm (GA) [32,33] to perform the optimization at the approximated surfaces. A general description of adaptive response surface methods is given in [30,31]. The parameters and details of the applied optimization algorithm are given in the following.

The adaptive response surface method is based on a panning parameter of 1.0, and an oscillation and zooming parameter of 0.6. The response surface is approximated by linear regression polynomials, whereas the supporting points are defined by a D-optimal quadratic design-of-experiment (DOE) scheme. The response surface is changed adaptively depending on the problem. The optimization on the response surface is performed by a genetic algorithm. As the convergence of the genetic algorithm near the optimum is poor and no unique solution can be found, when using several runs, a subsequent application of the gradient-based algorithm refines the optimum on the response surface obtained by the genetic algorithm. For the genetic algorithm, a population of 10 individuals is used within each of the 15 generations, whereas one individual is used as elite and one individual will be replaced. The crossover rate is 50 percent and the selection pressure is 90 percent. The cliff value is set to 20. The gradient-based method uses the SQP (NLPQL) approach [39]. The NLPQL algorithm stops after 50 iterations or 50 function calls and the gradients are calculated using central differences. As the optimization is done on a response surface defined by linear polynomials, the criterion of differentiable objective for the SQP algorithm is guaranteed.

## Appendix B. Spearman correlation coefficient

The Pearson correlation coefficient [40,41] between two sets of data  $x_i$  and  $y_i \forall i = 1, 2, \dots, n$  is defined as

$$r_{xy} = \frac{\sum_{i=1}^n (x_i - \bar{x})(y_i - \bar{y})}{\sqrt{\left(\sum_{i=1}^n (x_i - \bar{x})^2\right) \left(\sum_{i=1}^n (y_i - \bar{y})^2\right)}}. \quad (19)$$

$\bar{\bullet}$  denotes the mean value of the variables. As the coefficient only indicates the linear correlation between the two data sets  $x$  and  $y$ , a coefficient which describes a general monotonic correlation between the data has been introduced by Spearman [36]. The Spearman correlation coefficient [41,40]

$$r_{xy}^S = \frac{\sum_{i=1}^n (R(x_i) - \bar{R(x)})(R(y_i) - \bar{R(y)})}{\sqrt{\left(\sum_{i=1}^n (R(x_i) - \bar{R(x)})^2\right) \left(\sum_{i=1}^n (R(y_i) - \bar{R(y)})^2\right)}} \quad (20)$$

is similar to the Pearson correlation coefficient, but it uses rank coefficients of the data sets  $R(x_i)$  and  $R(y_i)$  instead of the data itself. The rank coefficients with values between 1 and  $n$  are assigned according to the ordering of the values  $x_i$  and  $y_i$ ,

independently for both data sets. Using  $D_i = R(x_i) - R(y_i)$ , Eq. (20) simplifies to [41]

$$r_{xy}^S = 1 - \frac{6 \sum_{i=1}^n D_i^2}{n(n^2-1)}. \quad (21)$$

Even though the Spearman correlation coefficient has been developed and applied within the field of social science, it is widely used in natural science and engineering. Applications are given, for example, in [38,37].

## References

- [1] M.I. Friswell, J.E. Mottershead, *Finite Element Model Updating in Structural Dynamics*, Kluwer Academic Publishers, Netherlands, 1995.
- [2] S. Doebling, F. Hemez, W. Rhee, Statistical model updating and validation applied to nonlinear transient structural dynamics, *European COST F3 Conference on System Identification and Structural Health Monitoring*, Madrid, Spain, 2000.
- [3] V. Zabel, M. Brehm, Stochastic model updating methods—a comparative study, *IMAC XXVII A Conference and Exposition on Structural Dynamics*, Orlando, FL, USA, 2009.
- [4] R. Cantieni, M. Brehm, V. Zabel, T. Rauert, B. Hoffmeister, Ambient testing and model updating of a filler beam bridge for high-speed trains, *Proceedings of 7th European Conference on Structural Dynamics (EURODYN)*, Southampton, UK, 2008.
- [5] D.J. Ewins, *Modal Testing—Theory Practice and Application*, second ed., Research Studies Press Ltd, 2000.
- [6] N.M.M. Maia, J.M.M. Silva (Eds.), *Theoretical and Experimental Modal Analysis*, Research Studies Press, Baldock, UK, 1997.
- [7] W. Heylen, S. Lammens, P. Sas, *Modal Analysis Theory and Testing*, second ed., Katholieke Universiteit Leuven, Leuven, Belgium, 1999.
- [8] R.J. Allemang, D.L. Brown, A correlation coefficient for modal vector analysis, *Proceedings of International Modal Analysis Conference*, 1982, pp. 110–116.
- [9] R.J. Allemang, The modal assurance criterion—twenty years of use and abuse, *Sound and Vibration* 37 (8) (2003) 14–21.
- [10] D.J. Ewins, Model validation: correlation for updating, *Proceedings of Indian Academy Sciences*, Vol. 25, Sadhana, 2000, pp. 221–246.
- [11] C. Morales, Comments on the MAC and the NCO, and a linear modal correlation coefficient, *Journal of Sound and Vibration* 282 (2005) 529–537.
- [12] T.S. Kim, Y.Y. Kim, Mac-based mode-tracking in structural topology optimization, *Computers and Structures* 74 (2000) 375–383.
- [13] T.P. Waters, Finite Element Model Updating using Measured Frequency Response Functions, PhD Thesis, University of Bristol, 1995.
- [14] N.A.J. Lieven, D.J. Ewins, Spatial correlation of mode shapes, the coordinate modal assurance criterion (COMAC), *Proceedings of International Modal Analysis Conference*, 1988.
- [15] D.L. Hunt, Application of an enhanced coordinate modal assurance criterion (ECOMAC), *Proceedings of International Modal Analysis Conference*, 1992, pp. 66–71.
- [16] N.A.J. Lieven, T.P. Waters, Error location using normalized orthogonality, *Proceedings of the 12th International Modal Analysis Conference*, Honolulu, 1994, pp. 761–764.
- [17] D. Ribeiro, R. Calçada, R. Delgado, M. Brehm, V. Zabel, Numerical and experimental assessment of the modal parameters of a bowstring arch railway bridge, *Proceedings of Experimental Vibration Analysis for Civil Engineering Structures (EVACES)*, Wroclaw, Poland, 2009.
- [18] Z.Y. Shi, S.S. Law, L.M. Zhang, Structural damage localization from modal strain energy change, *Journal of Sound and Vibration* 218 (5) (1998) 825–844.
- [19] Z.Y. Shi, S.S. Law, L.M. Zhang, Structural damage detection from modal strain energy change, *Journal of Engineering Mechanics* 126 (12) (2000) 1216–1223.
- [20] H. Li, H. Yang, S.-L.J. Hu, Modal strain energy decomposition method for damage localization in 3D frame structures, *Journal of Engineering Mechanics* 132 (9) (2006) 941–951.
- [21] P. Cornwell, S.W. Doebling, C.R. Farrar, Application of the strain energy damage detection method to plate-like structures, *Journal of Sound and Vibration* 224 (2) (1999) 259–374.
- [22] S.W. Doebling, F. Hemez, L.D. Peterson, C. Farhat, Improved damage location accuracy using strain energy-based mode selection criteria, *AIAA Journal* 35 (4) (1997) 693–699.
- [23] E. Reynders, G. de Roeck, P.G. Bakir, C. Sauvage, Damage identification on the Tiffel Bridge by vibration monitoring using optical fibre strain sensors, *Journal of Engineering Mechanics* 133 (2) (2007) 185–193.
- [24] S. Keye, Model Updating of Modal Parameters from Experimental Data and Applications in Aerospace, PhD Thesis, University of Greenwich, 2003.
- [25] J.E.T. Penny, M.I. Friswell, S.D. Garvey, Automatic choice of measurement location for dynamic testing, *AIAA Journal* 32 (1994) 407–414.
- [26] R.J. Guyan, Reduction of stiffness and mass matrices, *AIAA Journal* 3 (2) (1965) 380.
- [27] P. Avitabile, J. O'Callahan, J. Milani, Model correlation and orthogonality criteria, *Proceedings of 6th International Modal Analysis Conference (IMAC)*, Orlando, FL, USA, 1988, pp. 1039–1047.
- [28] J. O'Callahan, P. Avitabile, R. Riemer, System equivalent reduction expansion process (SEREP), *Proceedings of 7th International Modal Analysis Conference (IMAC)*, Las Vegas, NV, USA, 1989, pp. 29–37.
- [29] H.H. Khodaparast, J.E. Mottershead, M.I. Friswell, Perturbation methods for the estimation of parameter variability in stochastic model updating, *Mechanical Systems and Signal Processing* 22 (2008) 1751–1773.
- [30] L. Etman, J. Adriaens, M. van Slagmaat, A. Schoofs, Crashworthiness design optimization using multipoint sequential linear programming, *Structural Optimization* 12 (1996) 222–228.
- [31] H. Kurtaran, A. Eskandarin, D. Marzougui, N. Bedewi, Crashworthiness design optimization using response surface approximations, *Computational Mechanics* 29 (2002) 409–421.
- [32] J.H. Holland, *Adaptation in Natural and Artificial Systems—An Introductory Analysis with Applications to Biology, Control, and Artificial Intelligence*, MIT Press, 1992.
- [33] D.E. Goldberg, *Genetic Algorithms in Search, Optimization and Machine Learning*, Addison-Wesley Longman Publishing Co. Inc, Boston, MA, USA, 1989.
- [34] M. Brehm, V. Zabel, R. Cantieni, Modell Anpassung einer Eisenbahnbrücke für den Hochgeschwindigkeitsverkehr, *VDI-Berichte Nr. 2063-Baudynamik*, VDI Verlag GmbH, 2009, pp. 403–418.
- [35] R. Cantieni, M. Brehm, V. Zabel, T. Rauert, B. Hoffmeister, Ambient modal analysis and model updating of a twin composite filler beam railway bridge for high-speed trains with continuous ballast, *Proceedings of IMAC-XXVI Conference on Structural Dynamics*, Orlando, FL, USA, 2008.
- [36] C. Spearman, The proof and measurement of association between two things, *American Journal of Psychology* 15 (1904) 72–101.
- [37] C. Mares, J.E. Mottershead, M.I. Friswell, Stochastic model updating: part 1—theory and simulated example, *Mechanical Systems and Signal Processing* 20 (2006) 1674–1695.
- [38] J.E. Mottershead, C. Mares, S. James, M.I. Friswell, Stochastic model updating: part 2—application to a set of physical structures, *Mechanical Systems and Signal Processing* 20 (2006) 2171–2185.
- [39] K. Schittkowski, NLPQL: a fortran subroutine solving constrained nonlinear programming problems, *Annals of Operations Research* 5 (1985) 485–500.
- [40] R.V. Hogg, J.W. McKean, A.T. Craig, *Introduction to Mathematical Statistics*, sixth ed., Pearson Prentice Hall, 2005.
- [41] J. Hartung, B. Elpelt, *Multivariate Statistik*, seventh ed., R. Oldenbourg Verlag, 2007.